Heliyon 9 (2023) e16066

Contents lists available at ScienceDirect

Heliyon

journal homepage: www.cell.com/heliyon

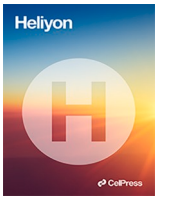

Research article

Absorption wavelength (TD-DFT) and adsorption of metal chalcogen clusters with methyl nicotinate: Structural, electronic, IRI, SERS, pharmacological and antiviral studies (HIV and omicron)

Sravanthi R [a,b], S. Mahalakshmi [a], V. Vetrivelan [c], Ahmad Irfan [d], S. Muthu [e,*]

[a] Department of Physics, Ethiraj College for Women, Chennai, 600008, Tamil Nadu, India
[b] University of Madras, Chennai, 600005, Tamil Nadu, India
[c] Department of Physics, Government College of Engineering, Srirangam, Trichy 620012, Tamil Nadu, India
[d] Department of Chemistry, College of Science, King Khalid University, P. O. Box 9004, Abha, 61413, Saudi Arabia
[e] Department of Physics, Arignar Anna Govt.Arts College, Cheyyar, 604407, Tamil Nadu, India

ARTICLE INFO

Keywords:
DFT
Electronic properties
SERS
Drug likeness
Molecular docking

ABSTRACT

The DFT B3LYP-LAND2DZ technique is used to examine interactions of Methyl nicotinate with copper selenide and zinc selenide clusters. The existence of reactive sites is determined using ESP maps and Fukui data. The energy variations between HOMO and LUMO are utilised to calculate various energy parameters. The Atoms in Molecules and ELF (Electron Localisation Function) maps are employed to investigate the topology of the molecule. The Interaction Region Indicator is used to determine the existence of non-covalent zones in the molecule. The UV–Vis spectrum using the TD-DFT method and DOS graphs are used to obtain the theoretical determination of electronic transition and properties. Structural analysis of the compound is obtained using theoretical IR spectra. To explore the adsorption of copper selenide and zinc selenide clusters on the Methyl nicotinate, the adsorption energy and theoretical SERS spectra are employed. Furthermore, pharmacological investigations are carried out to confirm the drug's non-toxicity. The compound's antiviral efficacy against HIV and Omicron is demonstrated via protein-ligand docking.

1. Introduction

The heterocyclic substance pyridine has the chemical formula C_6H_5N. Numerous natural substances, including vitamins, contain it. It has anti-inflammatory, anti-fungal, anti-amoebic and anti-microbial properties. Due to its biocompatibility, pyridine derivatives for a variety of human illnesses are widely available [1]. In addition to its biological function, it is utilised as a solvent in the textile, rubber and paint industries [2]. Methyl Nicotinate (MN) is a pyridine derivative and it is an ester that is produced from nicotinic acid and methanol. It has the chemical formula $C_7H_7NO_2$ and a molecular weight of 137.14 g/mol [3]. It has been chosen for the quantum chemical study and made to interact with the Copper Selenium (MNCS) and Zinc Selenium clusters (MNZS). Hosnedlova et al. stated that selenium nanoparticles have good bioavailability [4]. According to S. Zhang et al., selenium particles can be transmitted to cells

* Corresponding author.
E-mail address: mutgee@gmail.com (S. Muthu).

https://doi.org/10.1016/j.heliyon.2023.e16066
Received 27 February 2023; Received in revised form 27 April 2023; Accepted 4 May 2023
Available online 13 May 2023

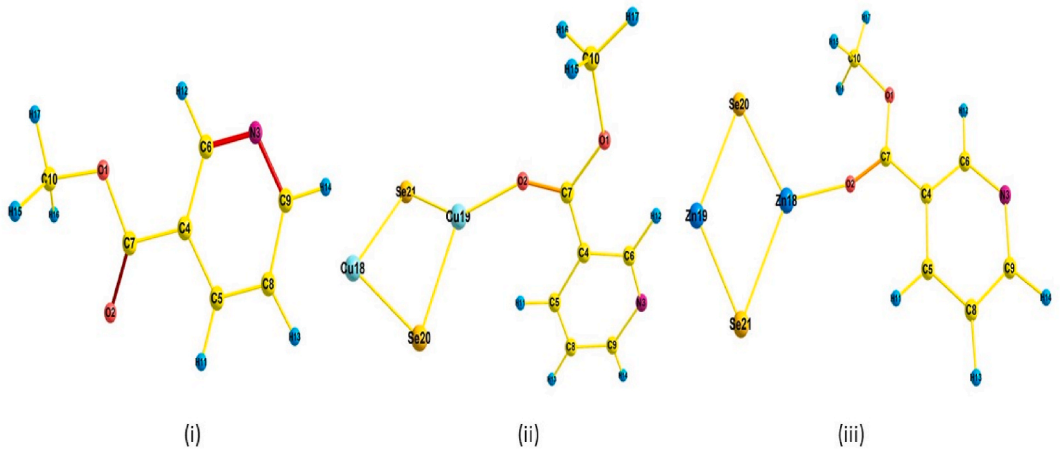

Fig. 1. Optimised structure of (i) MN (ii) MNCS and (iii) MNZS.

Table 1
Bond length (Å) of MN, MNCS and MNZS.

MN		MNCS		MNZS	
Bond length	Value	Bond length	Value	Bond length	Value
O1–C7	1.38	O1–C7	1.36	O1–C7	1.347
O1–C10	1.475	O1–C10	1.481	O1–C10	1.49
O2–C7	1.246	O2–C7	1.261	O2–C7	1.265
N3–C6	1.356	O2–Cu19	1.997	O2–Zn18	2.021
N3–C9	1.359	N3–C6	1.352	N3–C6	1.352
C4–C5	1.412	N3–C9	1.36	N3–C9	1.36
C4–C6	1.413	C4–C5	1.414	C4–C5	1.414
C4–C7	1.488	C4–C6	1.417	C4–C6	1.416
C5–C8	1.403	C4–C7	1.478	C4–C7	1.475
C5–H11	1.086	C5–C8	1.403	C5–C8	1.402
C6–H12	1.085	C5–H11	1.087	C5–H11	1.086
C8–C9	1.409	C6–H12	1.085	C6–H12	1.085
C8–H13	1.086	C8–C9	1.409	C8–C9	1.41
C9–H14	1.087	C8–H13	1.085	C8–H13	1.085
C10–H15	1.094	C9–H14	1.087	C9–H14	1.087
C10–H16	1.094	C10–H15	1.094	C10–H15	1.093
C10–H17	1.091	C10–H16	1.094	C10–H16	1.093
		C10–H17	1.09	C10–H17	1.089
		Cu18–Se20	2.348	Zn18–Se20	2.532
		Cu18–Se21	2.352	Zn18–Se21	2.514
		Cu19–Se20	2.423	Zn19–Se20	2.456
		Cu19–Se21	2.374	Zn19–Se21	2.457

and show a reduced DNA defilement reaction [5]. In addition, selenium contains antioxidant qualities that help build resistance to cancer [6,7]. J. Jansen et al. stated that zinc show mimics actions of the insulin [8]. Zinc has a favourable metabolism in both humans and animals [9]. Copper is a bioactive component which been employed in diagnostics and cures [10]. Nickel and cobalt selenides were shown to have cationic and anionic states, according to V. Nagarajan et al. [11]. The structural features and molecular characteristics of MN, MNCS and MNZS, are determined by a computational technique aided by DFT [12]. The morphology, kinematics, and electronic structures have all been computed in detail using DFT. The reactive regions are visualised via ESP and the molecule's chemical bonding is viewed using ELF. The Docking studies determine the biological parameter and additionally, features for toxicities and drug-likeness have been achieved.

2. Computational methods

The optimised structure of MN, MNCS and MNZS is obtained using the DFT method employed with B3LYP techniques [13] and LANL2DZ basis with the aid of Gaussian 09w [14]. ESP, FMO, NLO and Fukui evaluations are accomplished using the DFT approach. UV–Vis analysis uses the TD-DFT approach. Theoretical IR, Raman and SERS techniques are utilised to determine the interaction between molecules and clusters, along with their vibrational assignments. The IRI (Interaction Region Indicator), ELF (Electron Localisation Function), and AIM (Atoms in Molecule) studies are performed using the Multiwfn 3.7 [15] program. SWISSADME [16] is

Table 2
Bond angle (degrees) of MN, MNCS and MNZS.

MN		MNCS		MNZS	
Bond angle	Value	Bond angle	Value	Bond angle	Value
C7–O1–C10	116.8	C7–O1–C10	118.1	C7–O1–C10	119.7
O1–C7–O2	122.8	O1–C7–O2	120.4	O1–C7–O2	122.6
O1–C7–C4	112.5	O1–C7–C4	114	O1–C7–C4	114.8
O1–C10–H15	110.1	O1–C10–H15	109.8	O1–C10–H15	110
O1–C10–H16	110.1	O1–C10–H16	109.8	O1–C10–H16	109.8
O1–C10–H17	104.8	O1–C10–H17	104.5	O1–C10–H17	104.3
O2–C7–C4	124.7	C7–O2–Cu19	146.1	C7–O2–Zn19	163.6
C6–N3–C9	117.9	O2–C7–C4	125.6	O2–C7–C4	122.5
N3–C6–C4	122.9	O2–Cu19–Se20	129.7	O2–Zn18–Se20	121.6
N3–C6–H12	116.7	O2–Cu19–Se21	142.8	O2–Zn18–Se21	127.5
N3–C9–C8	123.2	C6–N3–C9	117.9	C6–N3–C9	117.9
N3–C9–H14	115.9	N3–C6–C4	122.9	N3–C6–C4	122.6
C5–C4–C6	118.6	N3–C6–H12	116.7	N3–C6–H12	116.7
C5–C4–C7	118.9	N3–C9–C8	123.2	N3–C9–C8	123.3
C4–C5–C8	118.8	N3–C9–H14	115.8	N3–C9–H14	115.8
C4–C5–H11	119.3	C5–C4–C6	118.6	C5–C4–C6	118.9
C6–C4–C7	122.5	C5–C4–C7	120.4	C5–C4–C7	119.4
C4–C6–H12	120.4	C4–C5–C8	118.6	C4–C5–C8	118.5
C8–C5–H11	121.9	C4–C5–H11	121.2	C4–C5–H11	120
C5–C8–C9	118.6	C6–C4–C7	121	C6–C4–C7	121.7
C5–C8–H13	121.2	C4–C6–H12	120.4	C4–C6–H12	120.6
C9–C8–H13	120.2	C8–C5–H11	120.2	C8–C5–H11	121.5
C8–C9–H14	120.9	C5–C8–C9	118.8	C5–C8–C9	118.6
H15–C10–H16	109.4	C5–C8–H13	120.8	C5–C8–H13	121.1
H15–C10–H17	111.2	C9–C8–H13	120.4	C9–C8–H13	120.2
H16–C10–H17	111.2	C8–C9–H14	121	C8–C9–H14	120.9
		H15–C10–H16	109.9	H15–C10–H16	109.9
		H15–C10–H17	111.4	H15–C10–H17	111.4
		H16–C10–H17	111.4	H16–C10–H17	111.3
		Se20–Cu18–Se21	88.6	Se20–Zn18–Se21	110.9
		Cu18–Se20–Cu19	83.8	Zn18–Se20–Cu19	66.6
		Cu18–Se21–Cu19	84.7	Cu18–Se21–Zn19	66.9
		Se20–Cu19–Se21	86.4	Se20–Zn19–Se21	115.5

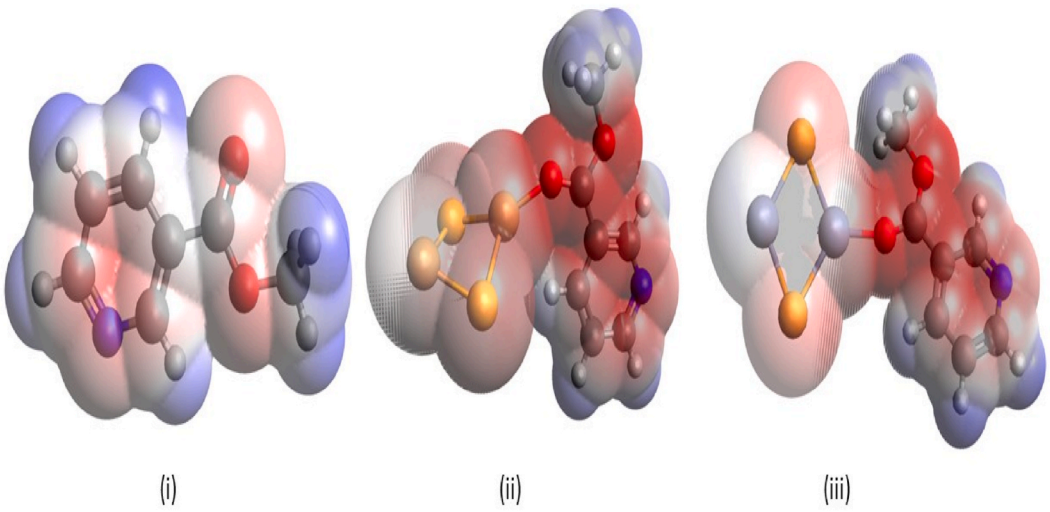

Fig. 2. ESP of (i) MN (ii) MNCS and (iii) MNZS

Table 3
Energy parameters of MN, MNCS and MNZS.

Parameter	MN	MNCS	MNZS
HOMO (eV)	−7.0815	−5.4056	−5.2939
LUMO (eV)	−2.0795	−3.6257	−3.3391
Ionization potential (eV)	7.0815	5.4056	5.2939
Energy gap (eV)	5.0019	1.7799	1.9548
Electronegativity-χ (eV)	4.5805	4.5157	4.3165
Chemical potential-μ (eV)	−4.5805	−4.5157	−4.3165
Chemical hardness-η (eV)	2.5010	0.8900	0.9774
Chemical softness-σ (eV)	0.1999	0.5618	0.5116
Electrophilicity index (eV)	4.1946	11.4562	9.5313
Adsorption Energy(kcal/mol)		−1.6626	−1.3348

employed to determine the compound's physicochemical activities. To dock the ligand with the selected proteins, PyRx software [17] is used.

3. Findings and discussions

3.1. Optimization of structure

The majority of quantum computational chemistry focuses on a molecular arrangement that heavily relies on geometry optimization [18]. MN, MNCS and MNZS are geometrically optimised by utilizing the LANL2DZ basis and the B3LYP approach. The CuSe and ZnSe clusters are made to interact with the MN. From Fig. 1, these clusters are placed nearer to the oxygen atom in the ester portion ($R–CO_2$-R^1) of MN [19]. In common MN, MNCS and MNZS have seven C–C bonds, five C–C bonds, three O–C bonds and two N–C bonds. Apart from this MNCS have one O–Cu bond and four Cu–Se bonds whereas MNZS have one O–Zn bond and four Zn–Se bonds. The observed maximum bond length for MN is at C4–C7, for MNCS is at Cu19–Se20 and for MNZS is at Zn18–Se20 signifies less electrostatic attraction between these atoms. The atoms with the shortest bonds exhibit greater electrostatic attraction to one another and for MN, MNCS and MNZS this is seen at C6–H12. The maximum bond angle observed for MN is at O2–C7–C4, for MNCS is at C7–O2–Cu19 and for MNZS is at C7–O2–Zn19 denoting high electronegativity with more stability due to less steric hindrance. The minimum bond angle signifies the repulsion of the molecules and for MN, MNCS and MNZS is at O1–C10–H17. This is due to the fact that lone pair-bond pair repulsion is higher in comparison with bond pair–bond pair repulsion. In comparison with MN, the MNCS and MNZS have maximum bond angles. Table 1 and Table 2 contain the bond details of MN, MNCS and MNZS.

3.2. ESP

The electrostatic potential maps produced by quantum mechanical computations explain the molecule's polarities and clearly depict them [20]. The colour-coded representations of the molecule's ESP make it simple to visualise. From Fig. 2, the red is designated to the anionic region, the blue is designated to the cationic region and the grey is designated to the neutral region [21]. In common, the majority of the positive zone is located near hydrogen atoms, the majority of the negative zone is found near oxygen atoms and the majority of the neutral zone is found near carbon atoms. In MNCS and MNZS the negative zone is found across the selenium atoms and the neutral zone is found across the copper and zinc atoms.

3.3. FMO and surface assimilation

The Molecular orbital (HOMO/LUMO) energy gap illustrates the electron transport interactions within the molecules [22]. The contributing molecule is referred to as HOMO and the recipient molecule is LUMO. The energy bandgap difference of MN, MNCS and MNZS is 5.001941, 1.77993 and 1.954842 eV. MNCS and MNZS have higher conductivity than MN because their MO energy difference is smaller. With the help of HOMO and LUMO energy difference values, μ,χ,η, σ [23] are calculated and tabulated in Table 3. The chemical softness of the MN (0.1999 eV) is low compared with the chemical softness of MNCS (0.5618 eV) and MNZS (0.5116 eV). As the softness of MN, MNCS, and MNZS decreases, they become chemically hard. The electrophilicity index of MN (4.1946) increases with the addition of Zn–Se clusters and Cu–Se clusters with MN. The electrophilicity of MNCS and MNZS is 11.4562 and 9.5313.

The adsorption is crucial for several operations on the surface. To identify the mechanistic basis in a compound, the adsorption energy is essential [24]. It is calculated by the formula $E_{Ads} = [E_{MN/(CS\ or\ Zs)} - (E_{MN} + E_{CS/ZS})]$.

$$E_{interaction} = -[E_{Ads}]$$

$E_{MN/\ (CS\ or\ ZS)}$, E_{MN} and $E_{CS/ZS}$ denote the total energy of the MNCS or MNZS complex, MN and CuSe and ZnSe clusters. The MNCS and MNZS have computed adsorption energies of −1.6626 and −1.3348 kcal/mol respectively. The higher binding energy of MNCS indicates that the adsorption is chemisorption, while the lower binding energy of MNZS indicates that the adsorption is physisorption [25].

Table 4
Fukui analysis of MN, MNCS and MNZS.

	MN				MNCS					MNZS				
Atoms	fr^+	fr^-	fr^0	Δf	Atoms	fr^+	fr^-	fr^0	Δf	Atoms	fr^+	fr^-	fr^0	Δf
1 O	−0.0274	−0.02165	−0.02453	−0.00575	**1 O**	−0.02668	−0.02219	−0.02443	−0.00448	**1 O**	−0.03887	−0.01992	−0.02939	−0.01895
2 O	−0.12274	−0.1289	−0.12582	0.006157	**2 O**	−0.00171	0.043802	0.021044	−0.04552	**2 O**	−0.07462	0.047068	−0.01378	−0.12169
3 N	−0.04278	−0.10268	−0.07273	0.059904	**3 N**	−0.02267	−0.02022	−0.02145	−0.00245	**3 N**	−0.02992	−0.01481	−0.02236	−0.01511
4 C	−0.03407	−0.02513	−0.0296	−0.00894	**4 C**	−0.0016	−0.00491	−0.00325	0.003305	**4 C**	−0.00327	−0.00353	−0.0034	0.000255
5 C	−0.11363	−0.07022	−0.09193	−0.04341	**5 C**	−0.02817	−0.01078	−0.01948	−0.01739	**5 C**	−0.07327	−0.0043	−0.03878	−0.06896
6 C	−0.08463	−0.10566	−0.09514	0.021033	**6 C**	−0.04003	−0.02091	−0.03047	−0.01911	**6 C**	−0.07153	−0.0144	−0.04296	−0.05713
7 C	−0.10139	−0.07269	−0.08704	−0.0287	**7 C**	−0.04596	−0.02027	−0.03311	−0.02569	**7 C**	−0.08646	−0.01323	−0.04984	−0.07324
8 C	−0.03922	−0.05854	−0.04888	0.019324	**8 C**	−0.01635	−0.01103	−0.01369	−0.00532	**8 C**	−0.02976	−0.00936	−0.01956	−0.0204
9 C	−0.12358	−0.10116	−0.11237	−0.02242	**9 C**	−0.04164	−0.01819	−0.02992	−0.02345	**9 C**	−0.08119	−0.01504	−0.04812	−0.06615
10 C	−0.01177	0.000978	−0.0054	−0.01275	**10 C**	−0.00365	−0.00089	−0.00227	−0.00275	**10 C**	−0.00249	−0.00016	−0.00133	−0.00233
11 H	−0.03499	−0.04076	−0.03788	0.005768	**11 H**	0.021259	0.055512	0.038386	−0.03425	**11 H**	−0.02091	0.023995	0.001545	−0.0449
12 H	−0.04363	−0.05926	−0.05144	0.015633	**12 H**	−0.01854	−0.013	−0.01577	−0.00555	**12 H**	−0.02878	−0.00602	−0.0174	−0.02276
13 H	−0.05756	−0.06096	−0.05926	0.003396	**13 H**	−0.01716	−0.00396	−0.01056	−0.0132	**13 H**	−0.0407	−0.00914	−0.02492	−0.03156
14 H	−0.06277	−0.07072	−0.06674	0.007945	**14 H**	−0.03024	−0.02098	−0.02561	−0.00927	**14 H**	−0.04746	−0.01738	−0.03242	−0.03008
15 H	−0.03034	−0.02548	−0.02791	−0.00486	**15 H**	−0.00923	−0.00077	−0.005	−0.00846	**15 H**	−0.01763	0.022103	0.002239	−0.03973
16 H	−0.03039	−0.02552	−0.02795	−0.00486	**16 H**	−0.00845	0.00011	−0.00417	−0.00856	**16 H**	−0.02354	0.014385	−0.00458	−0.03792
17 H	−0.03914	−0.03166	−0.0354	−0.00748	**17 H**	−0.02734	−0.0232	−0.02527	−0.00414	**17 H**	−0.03571	−0.03126	−0.03348	−0.00445
					18 Cu	−0.19499	−0.17259	−0.18379	−0.0224	**18 Zn**	0.021454	−0.13495	−0.05675	0.156399
					19 Cu	−0.1183	−0.14541	−0.13185	0.027113	**19 Zn**	−0.1705	−0.14564	−0.15807	−0.02486
					20 Se	−0.18106	−0.29796	−0.23951	0.116894	**20 Se**	−0.0684	−0.33484	−0.20162	0.266435
					21 Se	−0.18749	−0.29217	−0.23983	0.104682	**21 Se**	−0.07646	−0.33358	−0.20502	0.257119

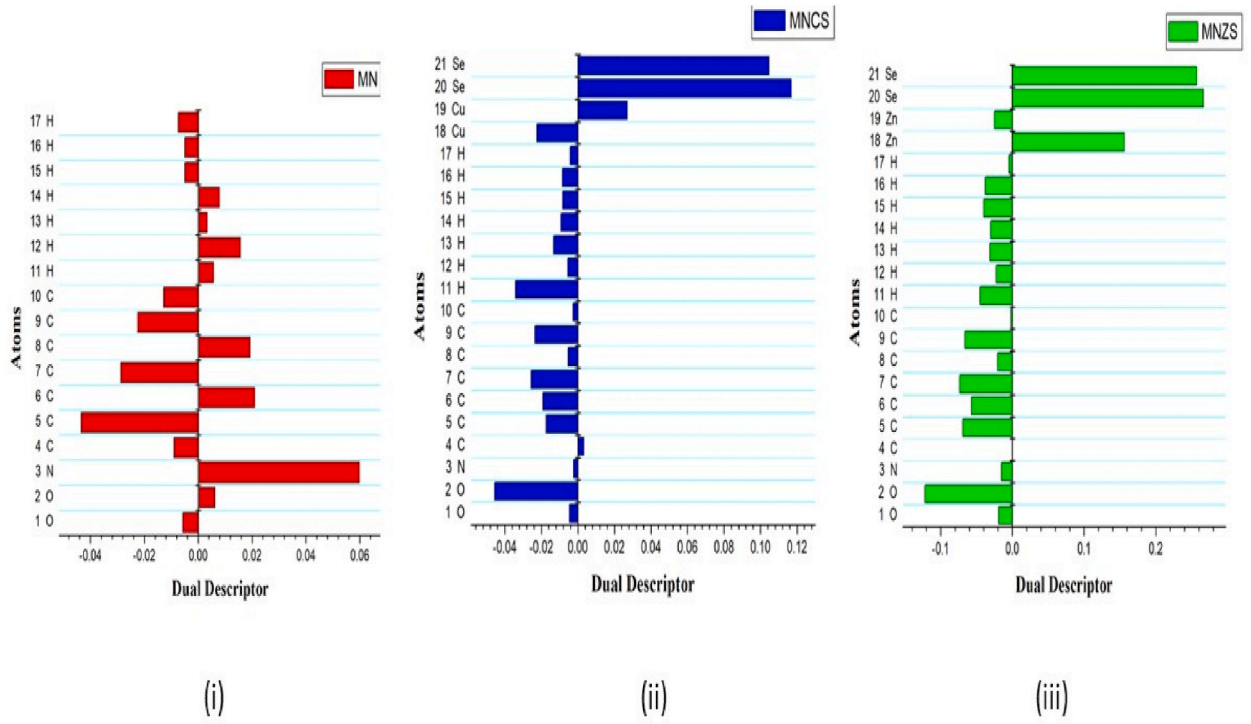

Fig. 3. Dual descriptor of (i) MN (ii) MNCS and (iii) MNZS

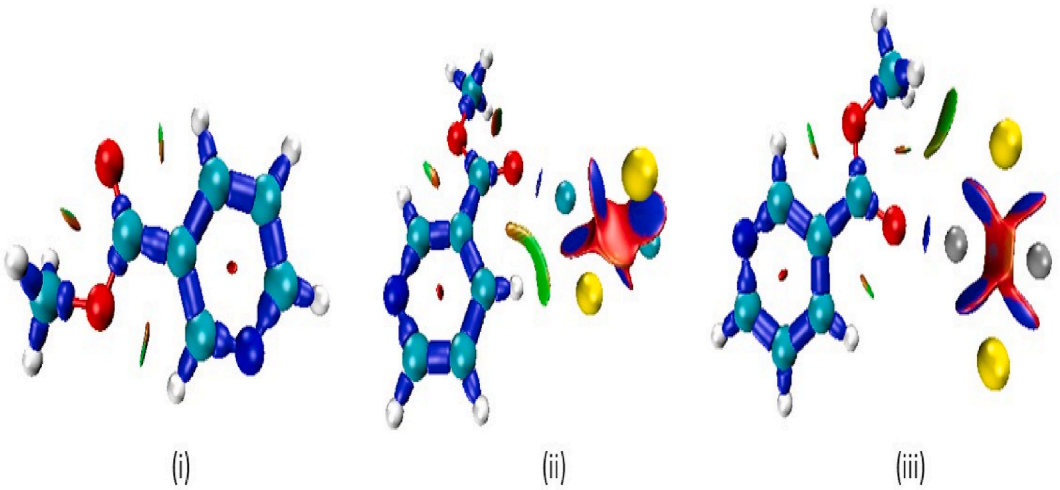

Fig. 4. IRI of (i) MN (ii) MNCS and (iii) MNZS

3.4. Determination of chemical reactivity

The Fukui function offers a framework for comprehending the mechanism of chemical processes by providing data on the reactivity regions inside the molecule. The electron-donating (nucleophile) and electron-accepting (electrophile) atoms can be easily identified. Each atom will be assigned have numbers under Mulliken charge analysis [26]. For the m^{th} atomic site's nucleophile f_m^+, electrophile f_m^- and radical f_m^0 attacks, the simplified Fukui functions are used.

$$f_m^+ = q_m(N) - q_m(N-1) \quad (1)$$

$$f_m^- = q_m(N+1) - q_m(N) \quad (2)$$

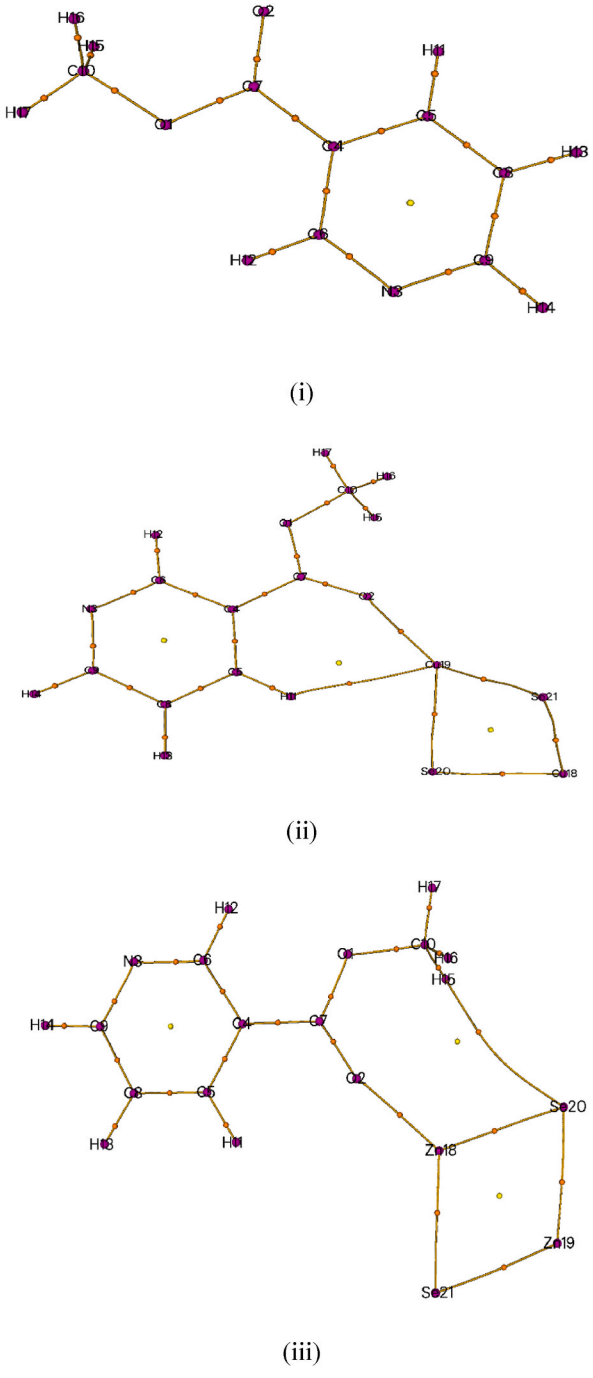

Fig. 5. Aim of (i) MN (ii) MNCS and (iii) MNZS

$$f_m^0 = \tfrac{1}{2}(q_m(N+1) - q_m(N-1)) \quad (3)$$

[27] The dual descriptor Δf can clearly identify truly nucleophilic and electrophilic areas and it can be defined as, $\Delta f = |f_m^{+} - f_m^{-}|$. The negative values ($\Delta f < 0$) for MN, MNCS, and MNZS are electrophile while the positive values ($\Delta f > 0$) are non-electrophile. From Table 4 and Fig. 3, the electrophilic sites (electron recipients) for MN are observed at O1, C4, C5, C7, C9, C10, H15, H16 and H17, for MNCS, they are observed at O1, O2, N3, C5, C6, C7, C8 C9, C10, H11, H12, H13, H14, H15, H16, H17 and Cu18 and MNZS, they are observed at O1, O2, N3, C5, C6, C7, C8 C9, C10, H11, H12, H13, H14, H15, H16, H17 and Zn19. The nucleophilic sites (electron donor) for MN are observed at N3, C6, C8, H11, H12, H13 and H14, for MNCS, they are observed at C4, Cu19, Se20 and Se21 and for MNZS, they are observed at C4, Zn18, Se20 and Se21 [28].

Table 5
Topological parameters of MN, MNCS and MNZS.

MN			MNCS			MNZS		
Atom	ρ (a. u)	$\nabla^2\rho$(a. u)	Atom	ρ (a.u)	$\nabla^2\rho$(a. u)	Atom	ρ (a. u)	$\nabla^2\rho$(a. u)
C9–N3	0.3045	−0.6821	**Se20–Cu18**	0.0625	0.1630	**Se20–Zn18**	0.0493	0.6824
C8–C9	0.2858	−0.7440	**Cu18–Se21**	0.0622	0.1602	**Zn18–Se21**	0.0508	0.6924
N3–C6	0.3063	−0.6886	**Se21–Cu19**	0.0608	0.1543	**Se21–Zn19**	0.0539	0.7620
C6–C4	0.2846	−0.7360	**Se20–Cu19**	0.0553	0.1399	**Se20–Zn19**	0.0538	0.7772
C4–C5	0.2848	−0.7487	**C9–N3**	0.0625	0.1630	**C9–N3**	0.3039	−0.6838
C8–C5	0.2877	−0.7653	**C8–C9**	0.2724	−0.9295	**C8–C9**	0.2856	−0.7440
C9–H14	0.2688	−0.8873	**N3–C6**	0.3090	−0.7011	**N3–C6**	0.3091	−0.7030
C8–H13	0.2656	−0.8589	**C6–C4**	0.0086	0.3051	**C6–C4**	0.2831	−0.7278
C5–H11	0.2682	−0.8955	**C4–C5**	0.2823	−0.7230	**C4–C5**	0.2835	−0.7415
O2–C7	0.3634	−0.5593	**C8–C5**	0.2883	−0.7692	**C8–C5**	0.2886	−0.7708
C7–C4	0.2496	−0.5588	**C9–H14**	0.2697	−0.8988	**C9–H14**	0.2700	−0.9036
C6–H12	0.2722	−0.9264	**C8–H13**	0.2669	−0.8761	**C8–H13**	0.2668	−0.8752
C7–O1	0.2670	−0.4471	**C5–H11**	0.2686	−0.9054	**C5–H11**	0.2687	−0.9054
O1–C10	0.2041	−0.2192	**H11–Cu19**	0.0092	0.2569	**C4–C7**	0.2550	−0.5860
C10–H15	0.2643	−0.8456	**Cu19–O2**	0.0660	0.5233	**Zn18–O2**	0.0593	0.3620
C10–H16	0.2642	−0.8455	**O2–C7**	0.3448	−0.4870	**O2–C7**	0.3398	−0.4777
C10–H17	0.2666	−0.8652	**C7–C4**	0.2533	−0.5770	**C6–H12**	0.2722	−0.9302
			C6–H12	0.2724	−0.9295	**C7–O1**	0.2863	−0.5049
			C7–O1	0.2789	−0.4893	**O1–C10**	0.1913	0.1436
			O1–C10	0.1983	−0.1829	**C10–H16**	0.2658	−0.8686
			C10–H15	0.2651	−0.8576	**C10–H17**	0.2686	−0.8924
			C10–H16	0.2651	−0.8571	**C10–H15**	0.2663	−0.8756
			C10–H17	0.2679	−0.8816	**H15–Se20**	0.0044	0.1355

3.5. Interaction Region Indicator (IRI)

In molecular systems, inter-atomic interactions are frequent. IRI is extremely useful in the study of many molecular structures and chemical reactions since it can detect molecule's weaker interactions zone. IRI is effective in identifying chemical bonds that are present in the molecules and it depends on the electron density [29]. The presence of covalent and non-covalent bonds present in MN, MNCS and MNZS are indicated using the IRI isosurface. From Fig. 4, blue isosurfaces indicate a zone of high electron density that strengthens the bond, green isosurfaces indicate a zone of weak interaction, and red isosurfaces indicate the steric effect or repulsion. The strong interactions are observed due to π-electrons conjunction within the aromatic ring i.e., for the C═C link. Repulsion (steric effect) is exhibited for the C—O link and the Van der Waals interactions are found between the hydrogen and metal (Cu and Zn) atoms [30].

3.6. Atoms in molecule

Quantum theory is used to describe the atom and its characteristics. The atom's actions are simply mirrored and conveniently summarised by the bonding pathways and the arrangement they define. The AIM concept was the first application of the topology analysis technique that Bader suggested for studying electron density. The eigenvalues of the Hessian matrix for electron density explain the CPs (Critical points). The CPs are sites in topography study terminology where $\nabla\rho$. $\vec{n} = 0$ [31] and it can be divided into four categories, BCP -bond (3, −1), RCP-ring (3, +1), NCP - nuclear (3, −3) and CCP -cage (3, +3). In Fig. 5, the yellow, magenta and orange spheres correspond to (3, −1), (3, −3) and (3, +1) [32]. CP index values are marked with cyan and the bond positions are shown by brown lines. In Table 5, the topology features ρ (e^- density) and $\nabla^2\rho$ (Laplacian e^- density) are listed. If $\nabla^2\rho < 0$ indicates the high electron concentration and $\nabla^2\rho > 0$ denotes electron exhaustion [33].

3.7. ELF

The electron localisation function (ELF) was developed as a technique to pinpoint areas in molecules and atoms where electrons get localised. Molecular and solid-state chemical bonding have both been extensively studied using this method [34]. Multiwfn 3.7 software is utilised to obtain the ELF images. The colour markers for ELF images span from blue to red and the range runs from 0.0 to 1.0 and from 0.5 to 1.0. The localised electron region with bonds and without bonds is visible in the range of 0.5–1.0 and the delocalized electronic region is visible in the range <0.5 [35]. According to Fig. 6, the electron depletion zones for MN are at C5, C8, C9, C10 and O2, for MNCS they are at C4 and N3 and for MNZS they are at C4, C7, C10, O1, O2, Zn18 and Se21 [36]. The electron concentration zones for MN are at H11, H13 and H14, for MNCS, they are at C6, H11 and H12 and for MNZS, they are at H12 and H17.

3.8. NLO

Non-Linear Optics studies show electric and magnetic fields interact with materials to create new fields that differ from the original

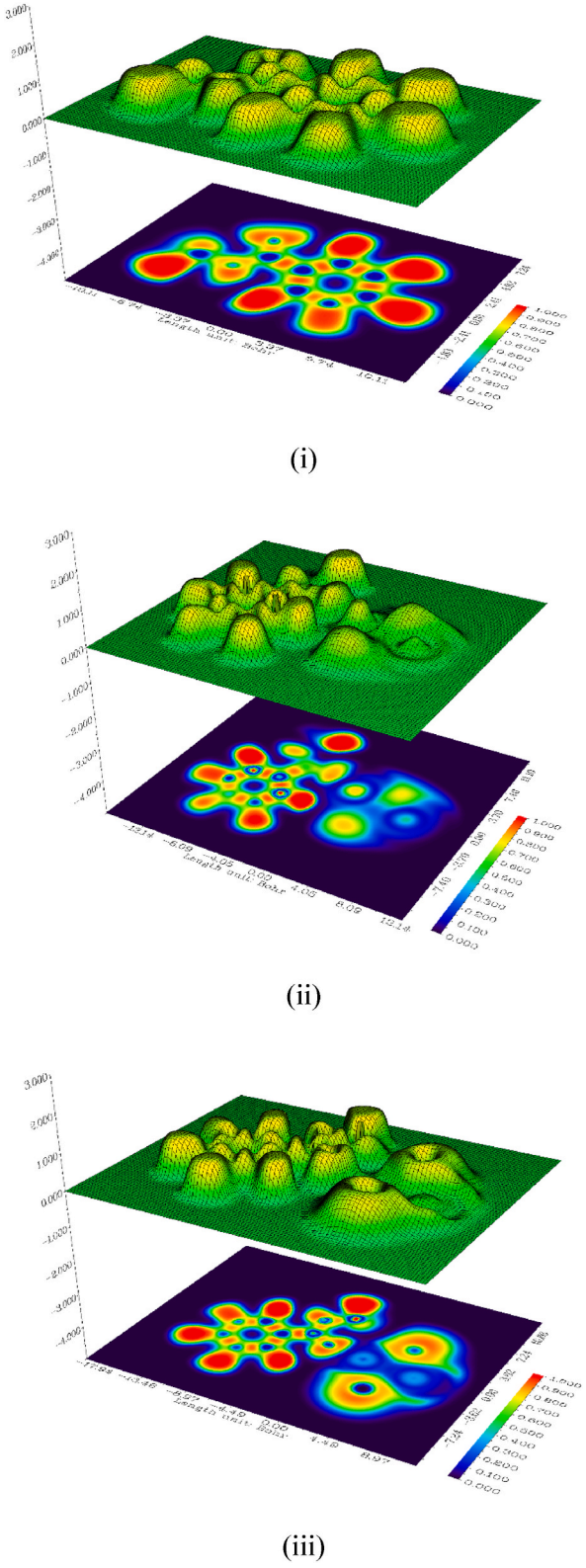

Fig. 6. ELF of (i) MN (ii) MNCS and (iii) MNZS

Table 6
NLO parameters of MN, MNCS and MNZS.

Parameters	MN	MNCS	MNZS
μ_x (D)	−0.2207339	−1.0287281	−2.0356542
μ_y (D)	0.2118868	0.9779263	0.3481454
μ_z (D)	0.0000695	−0.6519423	0.0523009
μ (D)	0.305972998	1.561937936	2.06587236
α_{xx} (e.s.u)	17.69289844	38.47605637	38.77543129
α_{yy} (e.s.u)	0.147546379	0.855707556	1.714605517
α_{zz} (e.s.u)	12.82197414	27.93442954	33.54534079
< α > (e.s.u)	$10.22080632 \times 10^{-24}$	$22.42206449 \times 10^{-24}$	$24.6784592 \times 10^{-24}$
Δα (e.s.u)	$149.7012495 \times 10^{-24}$	$320.7559079 \times 10^{-24}$	$331.5318974 \times 10^{-24}$
β_{xxx} (e.s.u)	−2504.373111	−34151.852	−10982.139
β_{xyy} (e.s.u)	941.513322	3172.2332	6447.7322
β_{xzz} (e.s.u)	361.0228649	2558.0791	−340.75498
β_{yyy} (e.s.u)	−43.11949082	3057.2877	−283.19173
β_{xxy} (e.s.u)	1.167178142	−2209.5758	182.61052
β_{yzz} (e.s.u)	−0.862064213	−1084.6872	47.307529
β_{zzz} (e.s.u)	−4.341579556	−1233.9971	−1.1977732
β_{xxz} (e.s.u)	−75.5510847	1656.4746	484.94492
β_{yyz} (e.s.u)	18.24035955	1080.4347	−109.82391
<β> (e.s.u)	$1.204178587 \times 10^{-30}$	$28.462235 \times 10^{-30}$	$4.8897707 \times 10^{-30}$

Table 7
Theoretical electronic parameters of MN, MNCS and MNZS.

System	Energy (cm^{-1})	Wavelength (nm)	Band gap	Osc. Strength	Symmetry	Major contributions
MN	31079.76837	321.7527197	3.853891278	0.0005	Singlet-A	HOMO- > LUMO (98%)
	36908.73723	270.9385569	4.576683416	0.0002	Singlet-A	H-2- > LUMO (94%)
	37153.92977	269.150533	4.607087292	0.0045	Singlet-A	HOMO- > L+1 (99%)
MNCS	5589.422193	1789.093694	0.693088352	0.0003	Singlet-A	HOMO- > LUMO (103%)
	10698.13795	934.7421065	1.326569105	0.0028	Singlet-A	H-1- > LUMO (99%)
	12036.21174	830.8261945	1.492490256	0.0047	Singlet-A	H-2- > LUMO (96%)
MNZS	11724.07518	852.9457417	1.453785322	0.001	Singlet-A	HOMO- > LUMO (100%)
	15726.19826	635.881593	1.950048584	0	Singlet-A	HOMO- > L+1 (98%)
	16091.56741	621.4435016	1.995354359	0.0002	Singlet-A	H-1- > LUMO (98%)

fields in terms of their amplitude, wavelength, optical effects and so on. It aids in comprehending the underlying physical processes that control molecules α (polarizability) and β (hyperpolarizability) [37]. NLO is in the limelight for the latest research since they are employed in many optical devices and modern technologies such as communication, sensors, and so on [38]. The μ (dipole moment), α and β values are listed in Table 6 and the results are compared with the prototype urea [39]. The μ of MN, MNCS and MNZS are found to be 0.30597, 1.56193 and 2.0658 D. The β of MN, MNCS and MNZS are found to be $1.204178587 \times 10^{-30}$, $28.462235 \times 10^{-30}$ and $4.8897707 \times 10^{-30}$ e.s.u. The μ and β of MN, MNCS and MNZS are greater when it is compared with the μ (1.3732 D) and β (0.3728 37 $\times 10^{-30}$ e.s.u) of the urea. Thus, we can infer that the title compound is a promising candidate for future nonlinear optical characteristic research.

3.9. Electronic analysis

UV–Visible spectroscopy is used to predict the energy and stability characteristics of molecules in their higher states [40]. Utilizing the TD-DFT approach, the UV–Visible spectrum of MN, MNCS and MNZS are generated theoretically using B3LYP- LANL2DZ technique. The absorption wavelength and excitation energies were the main factors influencing electronic transitions and HOMO-LUMO assignments are listed in Table 7. From Fig. 7, the absorption wavelength of MN is 321 nm, which is considerably shorter than the wavelengths of MNCS (1789 nm) and MNZS (852 nm) [41]. Because of the existence of metal chalcogen clusters, MNCS and MNZS exhibit a redshift. The wavelengths of the MNCS and MNZS absorbance maxima represent the charge-transfer spectra.

The DOS spectrum of the compound is used to obtain the electrical characteristics. From Fig. 8, the blue curve indicates the DOS spectrum and the small red and green vertical lines indicate the occupied and virtual orbitals [42]. The end of the vertical green line and the start of the vertical red line indicates the MO energy difference. The value of the band gap acquired in DOS agrees with the band gap values obtained in UV–Vis and Molecular Orbital investigations. The HOMO-LUMO transitions for MN are at −7.0815 and −2.0795 eV, for MNCS are at −5.4056 and −3.6257 eV and for MNZS are at −5.2939 and −3.3391 eV. Consequently, the DOS diagram depicts the molecule's HOMO-LUMO transition.

3.10. IR spectra

IR spectroscopy is a useful technique to determine the existence of specific functional groups in a molecule [43]. The IR spectrum

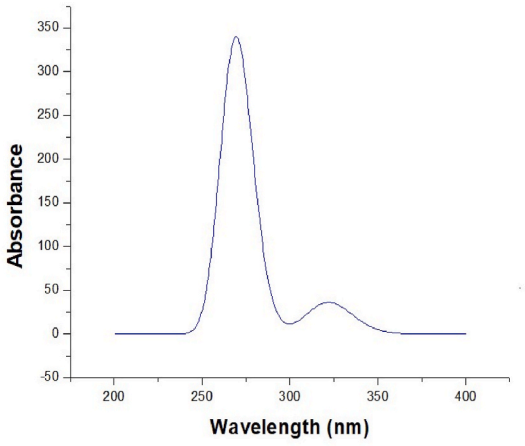

(i)

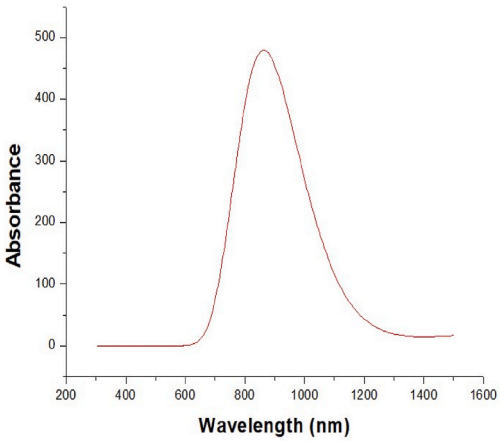

(ii)

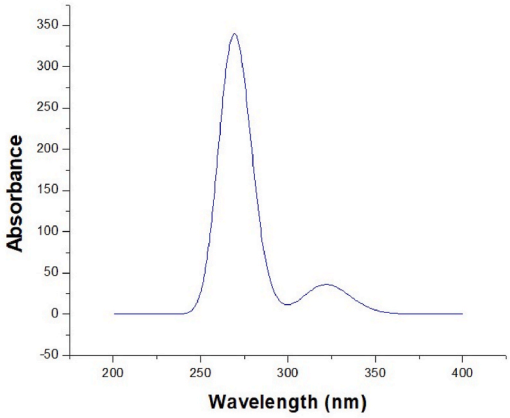

(iii)

Fig. 7. UV–Vis spectrum of (i) MN (ii) MNCS and (iii) MNZS

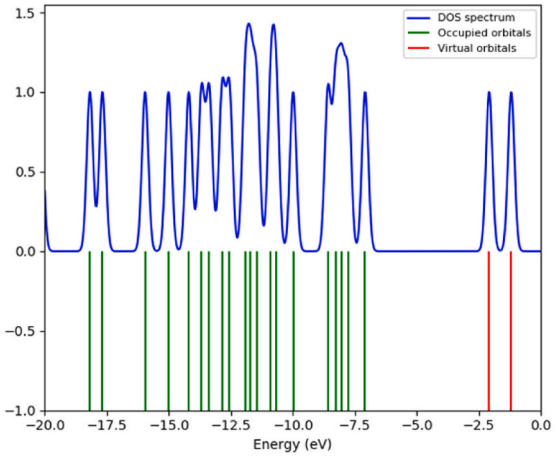

(i)

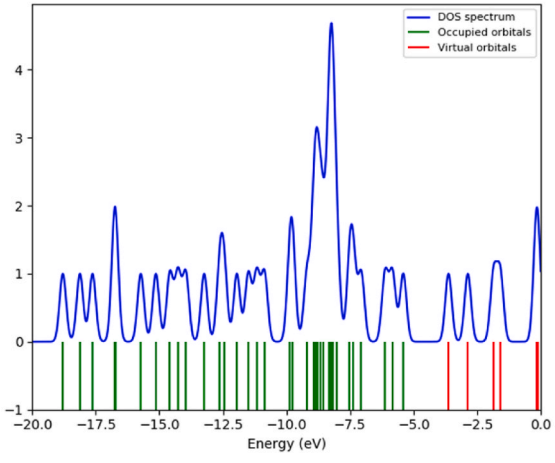

(ii)

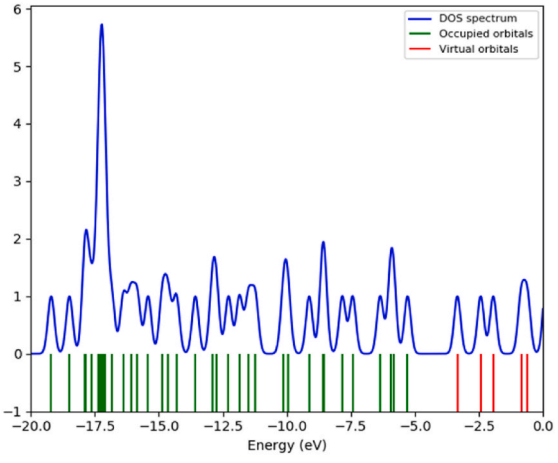

(iii)

(caption on next page)

Fig. 8. DOS of (i) MN (ii) MNCS and (iii) MNZS

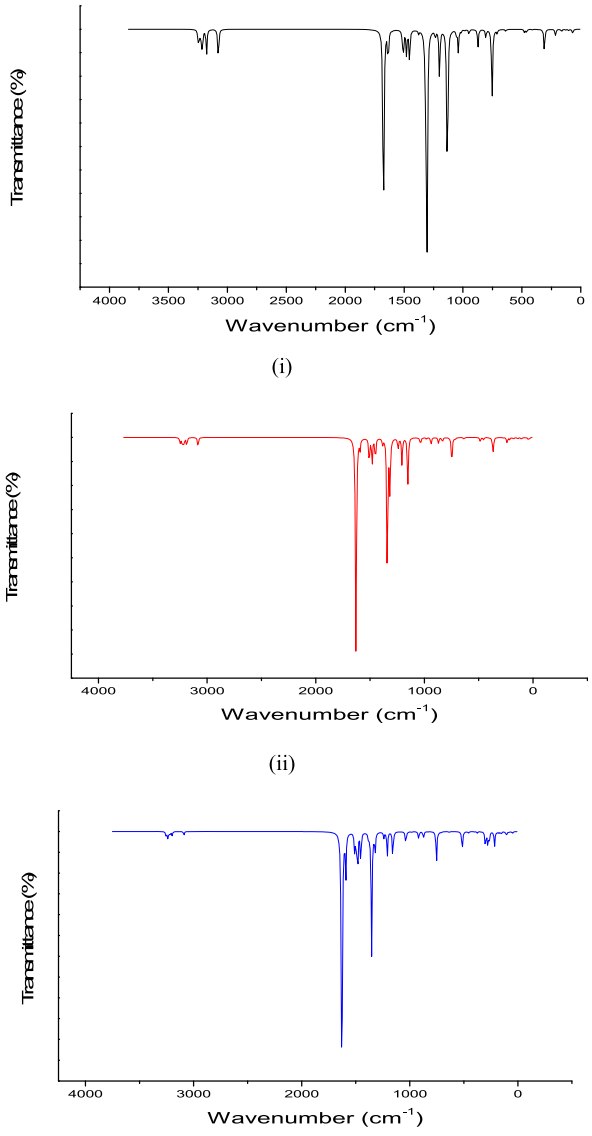

Fig. 9. Theoretical IR spectrum of (i) MN (ii) MNCS and (iii) MNZS

for MN, MNCS and MNZS has been theoretically obtained. The C–H vibrations occur at higher frequencies, because of its shorter bond length. The aromatic C–H vibrations for MN are observed at 3247, 3215, 3176 and 3075 cm^{-1}, for MNCS at 3249, 3227 and 3083 cm^{-1} and for MNZS at 3253, 3732 and 3218 cm^{-1}. Carbon bonds present in the compound have a higher influence on its aromatic ring and their vibrations are propagated within it. The C–C vibrations for MN are observed at 1631, 1502, 1315 1229, 800 and 360 cm^{-1}, for MNCS at 1625, 1504, 1336, 1312, 1237, 1146, 1030 and 829 cm^{-1} and for MNZS at 1629, 1587, 1449, 1316 and 1203 cm^{-1}. The carboxyl group is indicated by O–C stretching. The O–C vibrations for MN are observed at 1671 and 943 cm^{-1}, for MNCS at 933 cm^{-1} and for MNZS at 1623, 1349 and 912 cm^{-1}. Additionally, in MNCS, Cu–O vibrations are observed at 366 and 359 cm^{-1} and Cu–Se vibrations are observed at 234 cm^{-1}. In MNZS, Zn–O vibrations are observed at 508 and 259 cm^{-1} and Zn–Se vibrations are observed at 273 and 185 cm^{-1} (Fig. 9) [44].

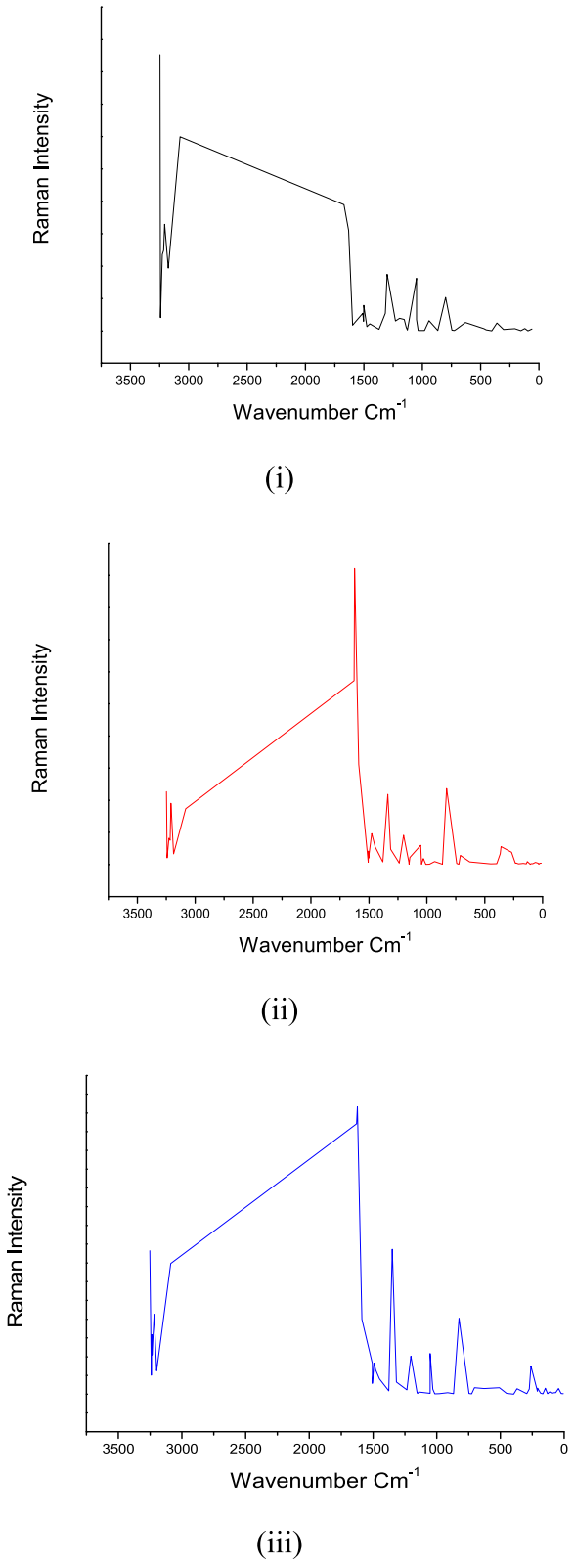

Fig. 10. (i) Raman spectrum of MN and SERS of (ii) MNCS and (iii) MNZS

Table 8
Raman and SERS spectrum.

MN				MNCS				MNZS
Wavenumber (cm^{-1})	Intensity	Wavenumber (cm^{-1})	Intensity	EF	Wavenumber (cm^{-1})	Intensity	EF	Assignments
3247	213.2391	3249	226.9192	6.42	3253	191.1547	10.36	**γCH**
3226	62.0862	3227	81.7527	31.68	3237	79.4074	27.90	**γCH**
3215	82.1643	3218	75.7195	7.84	3233	52.3775	36.25	**γCH**
3208	48.4722	3211	190.9049	293.84	3218	106.507	119.73	**γCH**
3075	97.3382	3083	173.2933	78.03	3088	174.0418	78.80	**γCH**
1631	4.5017	1628	572.0133	12606.61	1629	360.2928	7903.48	**γCC**
1502	19.6963	1504	41.9907	113.19	1506	40.9307	107.81	**βHCN**
1301	43.6445	1312	47.4111	8.63	1316	16.2202	62.84	**γCC**
1475	3.2097	1477	96.3823	2902.84	1478	32.102	900.16	**βHCH**
1371	1.2354	1379	8.1619	560.67	1376	4.4536	260.50	**βHCC**
1127	0.6803	1146	21.6927	3088.70	1145	1.4067	106.78	**γCC**
943	7.8375	933	8.8407	12.80	912	1.7956	77.09	**γOC**
800	25.9139	829	236.5391	812.79	825	101.2276	290.63	**γCC**
631	6.4855	630	8.4035	29.57	629	7.5077	15.76	**βCCC**

*γ - stretching, β - in-plane bending and EF – Enhancement factor.

Table 9
Drug likeness parameters of MN, MNCS and MNZS.

Descriptor		Value	
Parameters	MN	MNCS	MNZS
Hydrogen bond Donor (HBD)	0	0	0
Hydrogen bond Acceptor (HBA)	3	3	3
ALogP	0	0	0
Topological polar surface area (TPSA)	39.19	31.35	31.35
Molar refractivity	35.52	46.63	46.63
Number of atoms	16	22	22
Number of rotatable bonds	2	4	4
BBB	0.976524	1.74277	1.74277

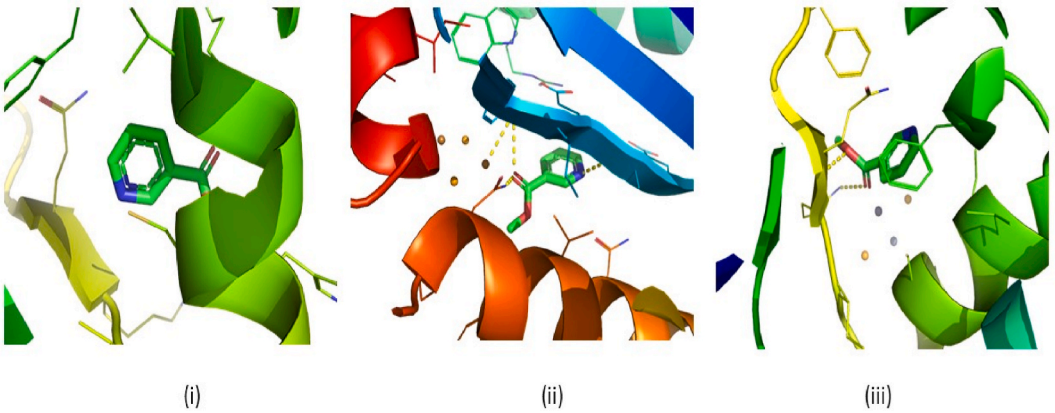

Fig. 11. 6L0C docked with (i) MN (ii) MNCS and (iii) MNZS.

3.11. Raman and SERS

The Raman and SERS were obtained to better understand the properties of the interactions between MN and metal chalcogen clusters (MNZS and MNCS) [45]. Raman spectra of MN have been theoretically observed at the range 3250-600 cm^{-1}. The most noticeable vibrations of Raman spectra for MN are the stretching vibrations of C–H, C–C and O–C. The maximum stretching observed for C–H at 3247, 3226, 3215, 3208 and 3075 cm^{-1} and for C–C is at 1631, 1301, 1127 and 800 cm^{-1}. The O–C vibrations indicate the presence of the carboxylic acid group and it is observed at 943 cm^{-1}. The existence of an amine group in the molecule is indicated by the presence of H–C–N bending. The H–C–H (1475 cm^{-1}), H–C–C (1371 cm^{-1}) and C–C–C (631 cm^{-1}) bending indicate that bending vibrations occur at the aromatic ring of the compound. For the MNCS and MNZS, the SERS have been acquired theoretically and from Fig. 10, the difference in the MN's Raman and SERS of MNCS and MNZS encompass most of the band's frequency shifting and

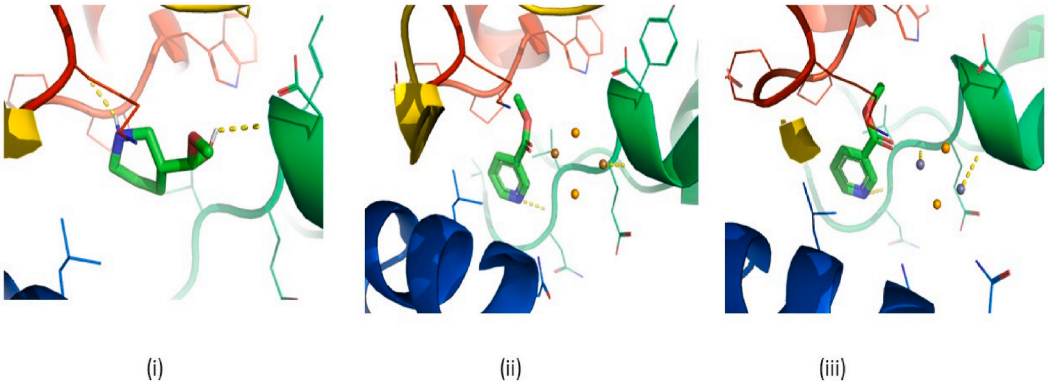

Fig. 12. 7U0N docked with (i) MN (ii) MNCS and (iii) MNZS.

Table 10
Molecular docking parameters of the proteins 6I0C and 7UON with MN, MNCS and MNZS.

Molecule	Protein	Bonded residues	Bond distance (Å)	Binding energy (kcal/mol)
MN	6L0C	TRP131	3.3	−4.3
		GLN137	3.3	
		CYS130	3.8	
		LYS127	5.4	
	7u0n	GLU564	2.2	−4.9
		ASP206	2.3	
		SER563	3.7	
		VAL209	4.4	
		PRO565	5.1	
		LEU95	5.0	
MNCS	6L0C	TYR83	3.2	−4.8
		ALA86	3.4	
		ASN184	3.2	
		GLU85	4.1	
	7u0n	GLU564	2.2	−4.9
		ASP206	2.3	
		SER563	3.7	
		VAL209	4.4	
		PRO565	5.1	
		LEU95	5.0	
MNZS	6L0C	GLN137	3.0	−4.6
		LYS136	3.8	
		PHE139	4.8	
		LYS127	5.2	
		CYS130	4.6	
	7u0n	GLU208	5.0	−5.6
		ASN210	3.1	
		ALA396	3.6	
		GLY205	2.7	
		LEU95	3.5	
		VAL209	4.8	
		TRP566	5.0	
		PRO565	4.9	

intensification [46]. When compared to typical Raman vibrations, C–H, C–C, and O–C stretching vibrations are found to have higher intensities in SERS. The C–H and C–C vibrations are found highly enhanced for MNCS with a red shift at 3211 cm^{-1} and with a blue shift at 1628 cm^{-1} and for MNZS with a redshift at 3218 and with a blue shift at 1629 cm^{-1}. The O–C vibrations are found highly enhanced for MNCS and MNZS at 912 cm^{-1} (Table 8). The H–C–H bending vibrations are enhanced and show a redshift at 1477 cm^{-1} (MNCS) and 1478 cm^{-1} (MNZS) and the H–C–C bending shows a good enhancement at the 1379 and 1376 cm^{-1} for MNCS and MNZS.

3.12. Pharmacological investigations

The drug-likeness notion offers suitable recommendations for preliminary-stage drug research. The most popular way that drug-likeness manifests itself is through the rules called Lipinski's Rule of Five [47]. The drug-like features are HBA and HBD range 5–10, log p =< 5, MR range 40–130 and TPSA range 0–140 Å [48]. Table 9 demonstrates that the values for MN, MNCS, and MNZS are

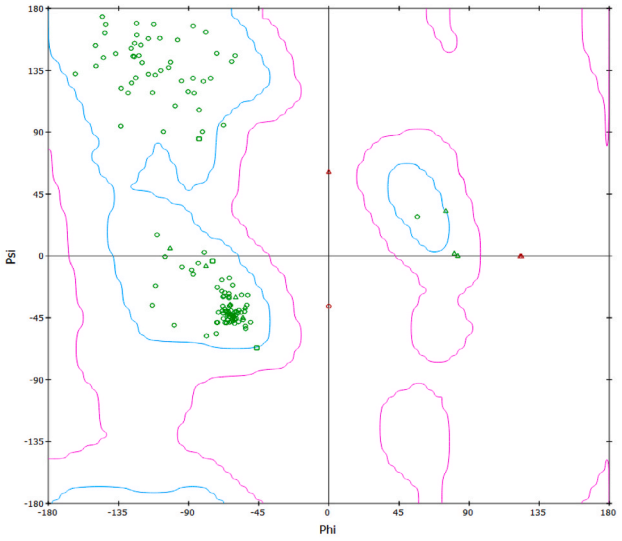

(i)

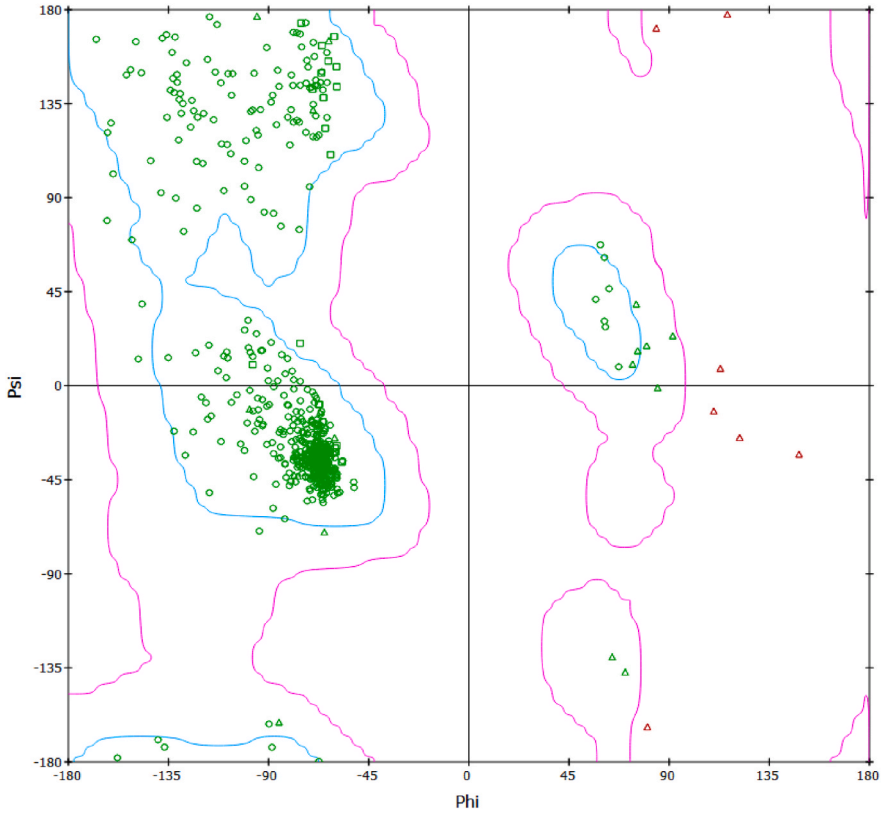

(ii)

(caption on next page)

Fig. 13. Ramachandran plot for the proteins (i) 6I0C and (ii) 7UON.

within the permitted ranges for the drug under consideration. Additionally, the molecules MN, MNCS, and MNZS have zero lipophilicity, indicating that they are between the aqueous and lipid phases [49]. The term blood-brain barrier (BBB) is used to refer to the special characteristics of the central nervous system to restrict undesirable components from entering the brain. The CNS-absorbing drug has a BBB score of >5 and non-CNS absorption has a BBB score of <5 [50]. The BBB score for the MN, MNCS, and MNZS is 0.976524, 1.7427, and 1.7427 respectively, indicating that they are non-CNS drugs.

3.13. In silico drug design

Computational approaches have gained prominence in the drug field of design by demonstrating their importance in the development of drugs. Numerous medicines which are now on the market for the treatment of various ailments were developed using computer modelling [51]. Docking is a computationally intensive approach for investigating ligand confirmations inside protein target sites [52]. The Lamarckian genetic algorithm and empirical free energy scoring function are used in PyRx software with the Autodock tool for the docking of flexible ligands and receptors. The compounds MN, MNCS and MNZS have been docked with the proteins 6L0C and 7U0N which are associated with HIV and omicron and displayed in Figs. 11 and 12 [53]. The binding energy and bonded amino acid residues with their distances are tabulated in Table 10. The receptor and ligand interactions are visualised using the PyMol application [54]. The 2D Ramachandran plots for the proteins 6L0C and 7U0N are obtained using Biovia Discovery Studio [55]. From Fig. 13, the Ramachandran plot's Φ and Ψ angles are used to evaluate the characteristics of the selected protein chains [56]. A large portion of the residues of amino acids of the proteins is in the permissible zone [57].

3.14. Conclusion

The structural features of MN, MNCS, and MNZS are produced using the LANL2DZ basis using Guassian09W. The energy band gap difference is calculated using FMO analysis. The IRI analysis is used to demonstrate the presence of non-covalent bonds. The Fukui and ESP diagrams are used to determine the existence of reactive sites, and electrophilic areas are identified around the oxygen and Selenium atoms. Topological properties have been determined using the ELF and AIM. UV–Vis is used to determining the electronic transitions within substances. According to NLO investigations, the compounds in consideration are optically active. Theoretical IR spectra are used to provide a structural study of the substance. The SERS demonstrate that the MNCS and MNZS have higher intensities than typical Raman. MN, MNCS, and MNZS satisfy the drug parameters and are docked with proteins 6L0C and 7U0N corresponding to HIV and omicron.

Author contribution statement

Sravanthi R: Conceived and designed the experiments; Performed the experiments; Analyzed and interpreted the data; Wrote the paper.

S Mahalakshmi: Performed the experiments; Analyzed and interpreted the data; Wrote the paper.

V Vetrivelan: Analyzed and interpreted the data.

Ahmad Irfan: Analyzed and interpreted the data; Contributed reagents, materials, analysis tools or data.

S Muthu: Conceived and designed the experiments; Contributed reagents, materials, analysis tools or data.

Data availability statement

Data will be made available on request.

Declaration of competing interest

The authors declare that they have no known competing financial interests or personal relationships that could have appeared to influence the work reported in this paper.

Acknowledgements

A. Irfan extends his appreciation to the Deanship of Scientific Research at King Khalid University for funding this work through Large Group Research Project under grant number RGP2/63/44.

References

[1] Role of Pyridines in Medicinal Chemistry and Design of BACE1 Inhibitors Possessing a Pyridine Scaffold, Yoshio Hamada, 2018, https://doi.org/10.5772/intechopen.74719.

[2] Pyridine and Pyridine Derivatives, 2000, https://doi.org/10.1002/0471238961.1625180919031809.a01.

[3] Norwegian Food Safety Authority (Mattilsynet), Methyl Nicotinate (MN) Risk Profile, 2012.

[4] Nano-selenium and its Nanomedicine Applications: a Critical Review, 2018, https://doi.org/10.2147/IJN.S157541.
[5] Encapsulation of Selenium in Chitosan Nanoparticles Improves Selenium Availability and Protects Cells from Selenium-Induced DNA Damage Response, 2011, https://doi.org/10.1016/j.jnutbio.2010.09.014.
[6] M. Kieliszek, Selenium–Fascinating microelement, properties and sources in food, Molecules 24 (7) (2019 Apr 3) 1298. PMID: 30987088; PMCID: PMC6480557.
[7] M. Kieliszek, S. Błażejak, Current knowledge on the importance of selenium in food for living organisms: a review, Molecules 21 (2016) 609, https://doi.org/10.3390/molecules21050609.
[8] J. Jansen, W. Karges, L. Rink, Zinc and diabetes–clinical links and molecular mechanisms, J. Nutr. Biochem. 20 (6) (2009 Jun) 399–417, https://doi.org/10.1016/j.jnutbio.2009.01.009.
[9] K.S. Siddiqi, A. ur Rahman, Tajuddin, et al., Properties of zinc oxide nanoparticles and their activity against microbes, Nanoscale Res. Lett. 13 (2018) 141, https://doi.org/10.1186/s11671-018-2532-3.
[10] Isidoros Iakovidis, Ioannis Delimaris, Stylianos M. Piperakis, The fundamental role of copper and the recognition of its complexes as important bioactive compounds, Molecular Biology International (2011) 2090–2182, https://doi.org/10.4061/2011/594529. Article ID 594529.
[11] V. Nagarajan, P. Gopinath, R. Chandiramouli, Structural stability and electronic properties of neutral, anionic and Ca selenide nanostructures: a DFT approach, Asian Journal of Applied Sciences 7 (2014) 721–728, https://doi.org/10.3923/ajaps.2014.721.728.
[12] M. Vennila, R. Rathikha, S. Muthu, A. Jeelani, Irfan Ahmad, Theoretical structural analysis (FT-IR, FT-R), solvent effect on electronic parameters NLO, FMO, NBO, MEP, UV (IEFPCM model), Fukui function evaluation with pharmacological analysis on methyl nicotinate, Computational and Theoretical Chemistry 1217 (2022), 113890, https://doi.org/10.1016/j.comptc.2022.113890.
[13] Djafri Ahmed, Fouzia Perveen, Nadia Benhalima, Nawel Khelloul, Rachida Rahmani, Ayada Djafri, Abdelkader Chouaih, Benali Kanoun Mohammed, Souraya Goumri-Said, Experimental spectral characterization, Hirshfeld surface analysis, DFT/TD-DFT calculations and docking studies of (2Z,5Z)-5-(4-nitrobenzylidene)-3-N(2-methoxyphenyl)-2-N'(2- methoxyphenylimino) thiazolidin-4-one, Heliyon 6 (Issue 12) (2020), e05754, https://doi.org/10.1016/j.heliyon.2020.e05754.
[14] M.J. Frisch, G.W. Trucks, H.B. Schlegel, et al., Gaussian 09, Revision A.02, Gaussian, Inc., Wallingford, CT, USA, 2009.
[15] Tian Lu, Feiwu Chen, Multiwfn, A multifunctional wavefunction analyzer, J. Comput. Chem. 33 (2012) 580–592, https://doi.org/10.1002/jcc.22885.
[16] SwissADME, A free web tool to evaluate pharmacokinetics, drug-likeness and medicinal chemistry friendliness of small molecules, Sci. Rep. 7 (2017), 42717.
[17] S. Dallakyan, A.J. Olson, Small-molecule library screening by docking with PyRx, Methods Mol. Biol. 1263 (2015) 243–250, https://doi.org/10.1007/978-1-4939-2269-7_19.
[18] H. Bernhard Schlegel, Geometrical optimization, Wiley Interdiscip. Rev. Comput. Mol. Sci. ume 1 (2011), https://doi.org/10.1002/wcms.34.
[19] Andrea Fabara, Sebastián Cuesta, Fernanda Pilaquinga, Lorena Meneses, Computational modeling of the interaction of silver nanoparticles with the lipid layer of the skin, Journal of Nanotechnology 2018 (2018) 1687–9503, https://doi.org/10.1155/2018/4927017. ID 4927017.
[20] A.J. Shusterman, L.M. Hoistad, Teaching chemistry with electron density models. 2. Can atomic charges adequately explain electrostatic potential maps? Chem. Educ. 6 (2001) 36–40, https://doi.org/10.1007/s00897000442a.
[21] P.K. Weiner, R. Langridge, J.M. Blaney, R. Schaefer, P.A. Kollman, Electrostatic potential molecular surfaces, Proc. Natl. Acad. Sci. U. S. A. 79 (12) (1982 Jun) 3754–3758.
[22] K. Rajalakshmi, DurgeshKumar Nayak, HOMO –LUMO analysis of dasatinib, Int. J. Mater. Struct. Integr. 12 (2017).
[23] R.G. Pearson, Chemical hardness and density functional theory, J. Chem. Sci. 117 (2005) 369–377, https://doi.org/10.1007/BF02708340.
[24] W. Gao, Y. Chen, B. Li, et al., Determining the adsorption energies of small molecules with the intrinsic properties of adsorbates and substrates, Nat. Commun. 11 (2020) 1196, https://doi.org/10.1038/s41467-020-14969-8.
[25] J.S. Al-Otaibi, Y.S. Mary, Y.S. Mary, et al., Adsorption of adipic acid in Al/B-N/P nanocages: DFT investigations, J. Mol. Model. 27 (2021) 113, https://doi.org/10.1007/s00894-021-04742-z.
[26] Apoorva Dwivedi, Vikas Baboo, Abhishek Bajpa, Fukui function analysis and optical, electronic, and vibrational properties of tetrahydrofuran and its derivatives: a complete quantum chemical study, Journal of Theoretical Chemistry 2015 (2015), 345234, https://doi.org/10.1155/2015/345234.
[27] Weitao. Yang, Wilfried J. Mortier, The use of global and local molecular parameters for the analysis of the gas-phase basicity of amines, Am. Chem. Soc. 108 (19) (1986) 5708–5711, https://doi.org/10.1021/ja00279a008.
[28] L.S. Anju, D. Aruldhas, I. Hubert Joe, S. Balachandran, Density functional theory, spectroscopic and hydrogen bonding analysis of fenoxycarb–water complexes, J. Mol. Struct. 1201 (2020), 127201, https://doi.org/10.1016/j.molstruc.2019.127201.
[29] E.R. Johnson, S. Keinan, P. Mori-Sánchez, J. Contreras-García, A.J. Cohen, W. Yang, J. Am. Chem. Soc. 132 (2010) 6498–6506, https://doi.org/10.1021/ja100936w.
[30] T. Lu, qinxue chen, Interaction region indicator (IRI): a very simple real space function clearly revealing both chemical bonds and weak interactions, Chem (2021), https://doi.org/10.26434/chemrxiv.13591142.v1.
[31] R.F.W. Bader, Atoms in molecules, Acc. Chem. Res. 18 (1985) 9–15, https://doi.org/10.1021/ar00109a003.
[32] F. Akman, N. Issaoui, A.S. Kazachenko, Intermolecular hydrogen bond interactions in the thiourea/water complexes (Thio-(H2O)n) (n = 1, ..., 5): X-ray, DFT, NBO, AIM, and RDG analyses, J.of Molec. Mod. 26 (6) (2020), https://doi.org/10.1007/s00894-020-04423-3.
[33] G. Bharathy, Johanan Christian Prasana, S. Muthu, Irfan Ahmad, Fazilath Basha Asif, A. Saral, S. Aayisha, R. Niranjana devi, Evaluation of electronic and biological interactions between N-[4-(Ethylsulfamoyl)phenyl]acetamide and some polar liquids (IEFPCM solvation model) with Fukui function and molecular docking analysis, J. Mol. Liq. 340 (2021), 117271, https://doi.org/10.1016/j.molliq.2021.117271.
[34] Priv Doz, Andreas Savin, Reinhard Nesper, Steffen Wengert, Thomas F. Fässler, ELF: the Electron Localization Function, 1997, pp. 1808–1832, https://doi.org/10.1002/anie.199718081.
[35] S. Selvakumari, C. Venkataraju, S. Muthu, Irfan Ahmad, A. Saral, Evaluation of electronic properties in different solvents, spectroscopic exposition (FT-IR, FT-Raman), and molecular docking studies of 5-Chloro-2-hydroxypyridine - insulysin inhibitor, J. Mol. Liq. 341 (2021), 117304, https://doi.org/10.1016/j.molliq.2021.117304.
[36] F.B. Asif, F.L.A. Khan, S. Muthu, M. Raja, Computational evaluation on molecular structure (Monomer, Dimer), RDG, ELF, electronic (HOMO-LUMO, MEP) properties, and spectroscopic profiling of 8-Quinolinesulfonamide with molecular docking studies, Comput. Theor. Chem. 1198 (2021), 113169, https://doi.org/10.1016/j.comptc.2021.113169.
[37] J. Jens Wolff, Rüdiger Wortmann, Organic materials for second-order non-linear optics, in: D. Bethell (Ed.), Advances in Physical Organic Chemistry, Academic Press, 1999, pp. 121–217, https://doi.org/10.1016/S0065-3160(08)60007-6.
[38] Elsa Garmire, Nonlinear optics in daily life, Opt Express 21 (2013) 30532–30544, https://doi.org/10.1364/OE.21.030532.
[39] P. Venkata Ramana, Sundius Tom, S. Muthu, K. Chandra Mouli, Y. Rama Krishna, K. Venkata Prasad, R. Niranjana Devi, Irfan Ahmad, C. Santhamma, Spectroscopic, quantum mechanical, electronic excitation properties (Ethanol solvent), DFT investigations and molecular docking analysis of an anti-cancer drug Bendamustine, J. Mol. Struct. 1253 (2022), 132211, https://doi.org/10.1016/j.molstruc.2021.132211.
[40] W. Mäntele, E. Deniz, UV-VIS absorption spectroscopy: lambert-Beer reloaded, Spectrochim. Acta Mol. Biomol. Spectrosc. 173 (2017 Feb 15) 965–968, https://doi.org/10.1016/j.saa.2016.09.037.
[41] M. Maria Julie, T. Prabhu, E. Elamuruguporchelvi, Fazilath Basha Asif, S. Muthu, Ahmad Irfan, Structural (monomer and dimer), wavefunctional, NCI analysis in aqueous phase, electronic and excited state properties in different solvent atmosphere of 3-{(E)-[(3,4-dichlorophenyl)imino]methyl} benzene-1,2-diol, J. Mol. Liq. 336 (2021), 116335, https://doi.org/10.1016/j.molliq.2021.116335.
[42] Harjinder Singh, Ashima Singh, J.M. Khurana, A combined experimental and theoretical approach for structural, spectroscopic, NLO, NBO, thermal and photophysical studies of new fluorescent 5-amino-1-(7-chloroquinolin-4-yl)-1H-1,2,3-triazole-4-carbonitrile using density functional theory, J. Mol. Struct. 1147 (2017) 725–734, https://doi.org/10.1016/j.molstruc.2017.07.010.

[43] M. Habib Rahuman, S. Muthu, B.R. Raajaraman, M. Raja, H. Umamahesvari, Investigations on 2-(4-Cyanophenylamino) acetic acid by FT-IR,FT-Raman, NMR and UV-Vis spectroscopy, DFT (NBO, HOMO-LUMO, MEP and Fukui function) and molecular docking studies, Heliyon 6 (Issue 9) (2020), e04976, https://doi.org/10.1016/j.heliyon.2020.e04976.
[44] Abdelali Boukaoud, Younes Chiba, Djamel Sebbar, A periodic DFT study of IR spectra of amino acids: an approach toward a better understanding of the N-H and O-H stretching regions, Vib. Spectrosc. 116 (2021), 103280, https://doi.org/10.1016/j.vibspec.2021.103280.
[45] Y.S. Mary, L. Ushakumari, B. Harikumar, et al., FT-IR, FT-Raman and SERS spectra of L-proline, JICS 6 (2009) 138–144, https://doi.org/10.1007/BF03246512.
[46] Guillermo Diaz Fleming, Justin J. Finnerty, Marcelo Campos-Vallette, Freddy Célis, Alvaro E. Aliaga, Carlos Fredes, Rainer Koch, Experimental and Theoretical Raman and Surface-Enhanced Raman Scattering Study of Cysteine, 2009, pp. 632–638, https://doi.org/10.1002/jrs.2175.
[47] G.R. Bickerton, G.V. Paolini, J. Besnard, S. Muresan, A.L. Hopkins, Quantifying the chemical beauty of drugs, Nat. Chem. 4 (2) (2012 Jan 24) 90–98.
[48] Christopher A. Lipinski, Franco Lombardo, Beryl W Dominy, Paul J. Feeney, Experimental and computational approaches to estimate solubility and permeability in drug discovery and development settings1PII of original article: S0169-409X(96)004231, Adv. Drug Deliv. Rev. 46 (Issues 1–3) (2001) 3–26, https://doi.org/10.1016/S0169-409X(00)00129-0.
[49] K. Sanjivanjit, Bhal, LogP—Making Sense of the Value, 2022, Advanced Chemistry Development, Inc, 2021.
[50] Mayuri Gupta, Hyeok Jun Lee, Christopher J. Barden, Donald F. Weaver, The blood–brain barrier (BBB) score, J. Med. Chem. 62 (21) (2019) 9824–9836, https://doi.org/10.1021/acs.jmedchem.9b01220.
[51] M.A. Phillips, M.A. Stewart, D.L. W.a. Xie, Has Molecular Docking Ever Brought us a Medicine? in: D.P. Vlachakis (Ed.), Molecular Docking IntechOpen, London, 2018 https://doi.org/10.5772/intechopen.72898.
[52] S.K. Kwofie, E. Broni, F.U. Yunus, J. Nsoh, D. Adoboe, W.A. Miller, M.D. Wilson, Molecular Docking Simulation Studies Identifies Potential Natural Product Derived-Antiwolbachial Compounds as Filaricides against Onchocerciasis, Biomedicines 9 (2021) 1682, https://doi.org/10.3390/biomedicines9111682.
[53] Jon Ainsley, Alessio Lodola, Adrian J. Mulholland, Christo Z. Christov, G. Tatyana, Karabencheva-Christova, Chapter One - Combined Quantum Mechanics and Molecular Mechanics Studies of Enzymatic Reaction Mechanisms, Advances in Protein Chemistry and Structural Biology 113 (2018) 1–32, https://doi.org/10.1016/bs.apcsb.2018.07.001.
[54] The PyMOL Molecular Graphics System, Version 1.2r3pre, Schrödinger, LLC, 2010.
[55] BIOVIA-Dassault Systemes, [Discovery Studio], Dassault Systèmes, San Diego, 2021.
[56] Umar Faruq Chowdhury, Abdullah Al Saba, , Abu Sufian Sufi, Akib Mahmud Khan, Ishrat Sharmin, Aziza Sultana, Md Ohedul Islam, Subtractive proteomics approach to Unravel the druggable proteins of the emerging pathogen Waddlia chondrophila and drug repositioning on its MurB protein, Heliyon 7 (Issue 6) (2021), e07320, https://doi.org/10.1016/j.heliyon.2021.e07320.
[57] Archana Pan, G. Pranavathiyani, Sibani Sen Chakraborty, Chapter 8 - Computational Modeling of Protein Three-Dimensional Structure: Methods and Resources, in: Molecular Docking for Computer-Aided Drug Design, Academic Press, 2021, pp. 155–178, https://doi.org/10.1016/B978-0-12-822312-3.00023-0.